Pressure-dependent surface viscosity and its surprising consequences in interfacial lubrication flows

Harishankar Manikantan and Todd M. Squires

Phys. Rev. Fluids **2**, 023301 — Published 9 February 2017

DOI: 10.1103/PhysRevFluids.2.023301

Pressure-dependent surface viscosity and its surprising consequences in interfacial lubrication flows

Harishankar Manikantan and Todd M. Squires
Department of Chemical Engineering, University of California, Santa Barbara, CA 93106-5080
(Dated: January 18, 2017)

The surface shear rheology of many insoluble surfactants depends strongly on the surface pressure (or concentration) of that surfactant. Here, we highlight the dramatic consequences that surface-pressure-dependent surface viscosities have on interfacially-dominant flows, by considering lubrication-style geometries within high Boussinesq (Bo) number flows. As with 3D lubrication, high-Bo surfactant flows through thin gaps give high surface pressures, which in turn increase the local surface viscosity, further amplifying lubrication stresses and surface pressures. Despite their strong nonlinearity, the governing equations are separable, so that results from 2D Newtonian lubrication analyses may be immediately adapted to treat surfactant monolayers with a general functional form of $\eta_s(\Pi)$. Three paradigmatic systems are analyzed to reveal qualitatively new features: a maximum, self-limiting value for surfactant fluxes and particle migration velocities appears for Π-thickening surfactants, and kinematic reversibility is broken for the journal bearing and for suspensions more generally.

I. INTRODUCTION

Complex interfaces occur in just about every technological application involving multiphase flows, be it in suspensions of bubbles, drops, and capsules; in films and coatings; or in foams and emulsions. The biological world is replete with high-interface materials as well, with striking examples found in microbial biofilms, alveolar interfaces in the lungs, and tear films. Surfactants play a crucial role in the formation, stability, and flow of these interfaces. The dynamics of such systems are both rich and important, with engineering applications ranging from reacting interfaces to enhanced oil recovery to microfluidic drop production.

Gradients in the interfacial surface tension, caused by changes in temperature or composition of the surfactant species, have long been known to drive so-called Marangoni flows [1, 2]. Marangoni stresses drive the evaporative instabilities responsible for 'tears of wine' [3], thermocapillary convection rolls [4], and the retardation of drop coalescence [5].

Certain surfactants exhibit surface rheological stresses when deforming against themselves, in addition to the well-known Marangoni stresses. While there have been disagreements over the origin or even existence of interfacial rheology, progress in measurement techniques specifically sensitive to in-plane, surface shear deformations of the interface have become increasingly reliable during recent decades [6–12], and reveal significant surface shear rheology in systems for which no Marangoni stresses should arise.

The Boussinesq-Scriven equations provide the now standard framework for coupling surface rheology to bulk fluid flows, and represent a momentum balance within the plane of the 2D surfactant monolayer, coupled to the subphase liquid via a viscous shear stress [13]. Excess viscous stresses within the interface are described by two surface viscosities – shear (η_s) and dilatational (κ_s) – just like in a three-dimensional fluid, along with gradients in the surface pressure Π. The surface pressure represents the surface stress exerted by the surfactant against the surface tension γ_0 inherent in the clean fluid interface,

$$\Pi(\Gamma) = \gamma_0 - \gamma(\Gamma), \tag{1}$$

and depends on the surfactant concentration Γ, according to an equation of state, $\Pi = \Pi(\Gamma)$.

Flows in such systems may be dominated by the interface or the subphase, depending on which exhibits greater resistance to deformation. The ratio of surface stresses to subphase stresses is generally given by the Boussinesq number,

$$\mathrm{Bo} = \frac{\eta_s}{\eta L}, \tag{2}$$

where η_s is the surface shear viscosity, η is the viscosity of the subphase, and L is a characteristic length scale over which gradients occur. We shall restrict our discussion to the $\mathrm{Bo} \gg 1$ limit, where the dynamics of particles in the monolayer are dominated by interfacial forces. In this limit, the interfacial layer behaves like two-dimensional Stokes flow, along with its subtleties and complexities – the most notorious being the Stokes paradox. Even though subphase drag plays only a subdominant role in the momentum balance at the interface, it ultimately regularizes the divergence at the root of the Stokes Paradox, as shown by Saffman and Delbruck for diffusion within lipid membranes

[14, 15]. Indeed, hydrodynamic coupling between particles diffusing within soap films transitions from 2D to 3D beyond a Boussinesq length scale [16]. Here we will consider surfactant monolayers that are bounded to remain within distances $|x| \ll \mathrm{Bo} \cdot L$; therefore, we assume subphase stresses to be negligible, so that the interface effectively behaves as a 2D continuum.

Three-dimensional fluids are typically approximated as incompressible; moreover, the viscosity of bulk fluids typically change appreciably only under extreme pressures [17–19]. 3D studies of such 'piezoviscous' liquids have used exponential and power-law $\eta(p)$ relations, particularly in the contexts of polymer melt processing[20, 21] and lubricating oils under exceedingly high pressures [22, 23]. Such flows may depart from the classical Newtonian solutions [22, 24] – *e.g.* the extrusion flux of polymer melts may slow dramatically under high pressures [21].

Surfactant monolayers, by contrast, are much easier to compress than their three-dimensional analogs. Such facile compression gives rise to significant qualitative differences in their flow response, beyond the introduction of surface dilatational viscous stresses. In particular, the surface viscosity η_s of most insoluble surfactants depends strongly on the surface pressure Π (or surface concentration) of that surfactant [6, 10, 25]. In fact, surface viscosity often increases exponentially with Π [25–27], increasing by orders of magnitude over relatively small increases in surface pressure Π.

The fact that surface viscosities can vary so dramatically, under conditions accessible to rather mundane flows, gives rise to a host of qualitatively new phenomena. To highlight these phenomena, and to build up physical intuition for such problems, we discuss a series of analytically tractable yet illustrative examples. We focus on lubrication geometries, whose thin gaps naturally amplify surface pressure variations, and thus accentuate the consequences of Π-dependent surface rheology. We show that many results from Newtonian lubrication analyses can be used directly in the Π-dependent surface rheology context, and that any functional form of $\eta_s(\Pi)$ may be treated by exploiting a remarkable separability in the nonlinear PDEs that govern the system. This separability allows results from 2D Newtonian lubrication studies to be immediately applied to arbitrary $\eta_s(\Pi)$ relations – *e.g.*taken directly from measurements, or using empirical relations (as is typically done in the 3D piezoviscous literature). Qualitative surprises emerge from this anaysis, including upper bounds on velocities and fluxes, and kinematic-reversibility-breaking. Such effects should be considered when designing and interpreting high-Bo flows and 2D suspensions.

II. PROBLEM FORMULATION

A. Quasi-Boussinesq approximation

We consider two-dimensional lubrication flows that occur within planar, insoluble surfactant monolayers (assumed to be flat, $z = 0$) atop a bulk fluid (Figure 1) that we assume obeys the (low-Re) Stokes equations,

$$\boldsymbol{\nabla} p = \eta \, \nabla^2 \mathbf{u}, \qquad \boldsymbol{\nabla} \cdot \mathbf{u} = 0, \tag{3}$$

where p, $\mathbf{u}$ and η are the pressure, velocity and shear viscosity of the bulk fluid. The quasi-steady Boussinesq-Scriven equations describe the interfacial stress balance at $z = 0$ [13]:

$$\boldsymbol{\nabla}_s \Pi = \boldsymbol{\nabla}_s \cdot (\eta_s(\boldsymbol{\nabla} \mathbf{u}_s + \boldsymbol{\nabla} \mathbf{u}_s^T)) + \boldsymbol{\nabla}_s[(\kappa_s - \eta_s)\boldsymbol{\nabla}_s \cdot \mathbf{u}_s] + \eta \left. \frac{\partial \mathbf{u}}{\partial z} \right|_{z=0} \tag{4}$$

where Π is the surface pressure, and η_s and κ_s are the two-dimensional shear and dilatational viscosities. Eq. 4 represent the equations of compressible, 2D viscous flow, with viscous stresses from the subphase exerting a body force within the surfactant monolayer. Non-dimensionalizing in the usual fashion,

$$\tilde{\boldsymbol{\nabla}}_s \tilde{\Pi} = \tilde{\boldsymbol{\nabla}}_s \cdot ((\tilde{\boldsymbol{\nabla}} \tilde{\mathbf{u}}_s + \tilde{\boldsymbol{\nabla}} \tilde{\mathbf{u}}_s^T)) + \tilde{\boldsymbol{\nabla}}_s \left[\left(\frac{\kappa_s}{\eta_s} - 1 \right) \tilde{\boldsymbol{\nabla}}_s \cdot \tilde{\mathbf{u}}_s \right] + \frac{1}{Bo} \left. \frac{\partial \tilde{\mathbf{u}}}{\partial \tilde{z}} \right|_{z=0}, \tag{5}$$

gives rise to the dimensionless (Boussinesq) number defined by Eq. (2). In the interfacially-dominated regime ($\mathrm{Bo} \gg 1$), subphase stresses are very small relative to surface rheological and surface pressure stresses. We assume the interface to remain planar, so that $\mathbf{u}_s \cdot \hat{\mathbf{z}} = 0$, and $\boldsymbol{\nabla}_s = (\mathbf{I} - \hat{\mathbf{z}}\hat{\mathbf{z}}) \cdot \boldsymbol{\nabla}$.

To incorporate Π-dependent viscosities into the governing equation (4), we follow the spirit of the Boussinesq approximation in Rayleigh-Bénard convection. In that context, changes in fluid viscosity and density due to temperature variations render the Navier-Stokes equations hopelessly nonlinear. Such variations, however, introduce only small perturbations to the inertial and viscous stresses, and can thus be neglected. Under the Boussinesq approximation, temperature-dependent density variations are only incorporated in the buoyant (gravitational) force, because it is only those variations that drive flows. By analogy, we approximate the surfactant interface as incompressible, so that the surface pressure Π acts to enforce incompressibility, but retain the Π-dependence of the surface viscosity

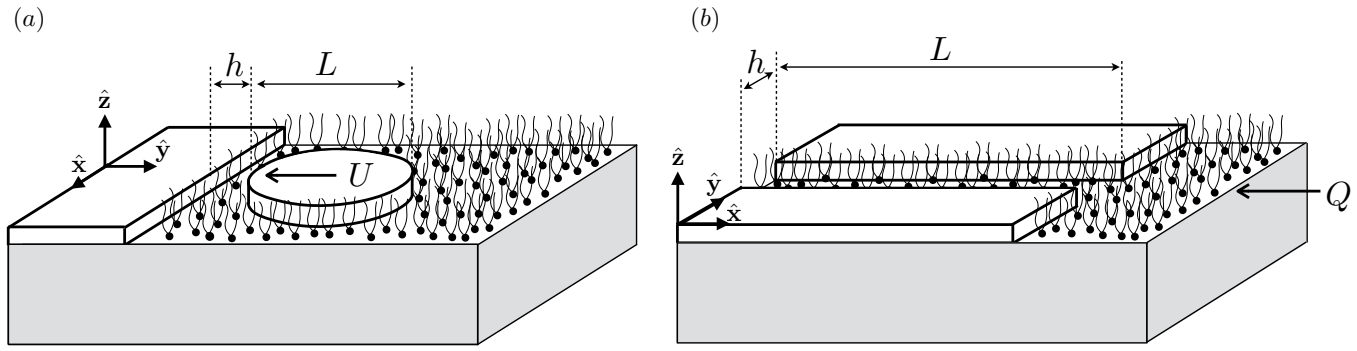

FIG. 1. Lubrication geometries within surfactant monolayers. Surface stresses due to interfacial rheology of the surfactant monolayer dominate over the viscous stresses from the subphase when Bo $\gg 1$, so that the surface flow is almost exclusively two-dimensional. When such surfactant monolayers flow within a thin gap of characteristic width h, much smaller than a macroscopic lengthscale L, the interfacial analog of standard (bulk) lubrication processes arise, shown here for (a) a disk approaching a wall, and (b) a monolayer driven through a narrow channel by a surface pressure gradient.

in the interfacial momentum equation. Fluid compressibility and surface dilatation are assumed to introduce small, quantitative changes to the flows – rather than the qualitative changes introduced by Π-dependent surface rheology. Appendix A discusses the validity of these approximations, which can also be checked *a posteriori*.

Within this quasi-Boussinesq framework, the interfacial momentum balance has Newtonian form, but with a Π-dependent surface viscosity η_s:

$$\boldsymbol{\nabla}_s \Pi = \boldsymbol{\nabla}_s \cdot [\eta_s(\Pi)(\boldsymbol{\nabla}\mathbf{u}_s + \boldsymbol{\nabla}\mathbf{u}_s^T)], \tag{6}$$

$$\boldsymbol{\nabla}_s \cdot \mathbf{u}_s = 0. \tag{7}$$

Unlike viscosities in three-dimensional liquids which are constant at all but extreme pressures, surface viscosities of surfactant monolayers change with surface pressure variations accessible over typical experiments. For many insoluble surfactants, the characteristic surface pressure change Π_c required for η_s to change appreciably is only a few mN/m. For example, the ubiquitous phospholipid Dipalmitoylphosphatidylcholine (DPPC) forms stable monolayers at air-water interfaces, and is a major constituent of pulmonary surfactant and lipid bilayer membranes. DPPC forms a liquid condensed phase above a critical surface pressure ($\sim 8\,$mN/m at room temperature), whose surface viscosity grows exponentially with Π [26–28], with surface pressure scale Π_c measured to be $\sim 6 - 8\,$mN/m. By contrast, eicosanol monolayers pressure-thin, as their tailgroups undergo a tilt-untilt transition (from an L2$'$ phase to an LS$_I$ phase [29]) as surface pressure increases, and η_s drops tenfold as Π increases from $\sim 8 - 15$ mN/m for $\Pi_c \sim 3$ mN/m, above which the surface viscosity plateaus [11, 25].

The exponential dependence of surface viscosity on surface pressure can be understood in terms of the free-area analog of classical free-volume theories of viscosity [27, 30–32]:

$$\eta_s^+(\Pi) = \eta_s^0 e^{(\Pi - \Pi_0)/\Pi_c}, \tag{8}$$

where the '+' indicates a Π-thickening surfactant, $\eta_s^0 = \eta_s(\Pi_0)$ is a reference viscosity at reference pressure Π_0, and Π_c is a pressure scale over which significant viscosity changes occur. For convenience, we will model pressure-thinning surfactants using an exponential relation similar to Eq. (8):

$$\eta_s^-(\Pi) = \eta_s^0 e^{-(\Pi - \Pi_0)/\Pi_c}. \tag{9}$$

Although these forms are analytically convenient, the results that follow can be extended to arbitrary $\eta_s(\Pi)$, *e.g.*, as measured experimentally.

B. Lubrication theory

Lubrication theory provides a straightforward framework to explore Π-dependent surface viscosity in an experimentally accessible regime, in geometries that accentuate its consequences. The analytical tractability of these lubrication problems highlights the qualitative differences introduced by Π-dependent surface viscosity.

The governing equations (6)-(7) differ from the conventional Boussinesq-Scriven equations (4) due to the Π-dependent surface shear viscosity $\eta_s(\Pi)$. We consider thin, slowly-varying 2D geometries, where a surfactant monolayer resides within the x-y plane (Figure 1) and flows with (2D) velocity $\mathbf{u}_s = (u, v)$. As is common with lubrication geometries, we consider gradients *along* the gap to occur over a lengthscale L that is large compared to the gap width h,

$$h = \epsilon L, \tag{10}$$

motivating the dimensionless quantities:

$$u = U\tilde{u}, \quad v = V\tilde{v}, \quad x = L\tilde{x}, \quad y = h\tilde{y}, \tag{11}$$

$$\Pi = \Pi_\ell \tilde{\Pi}, \quad \eta_s(\Pi) = \eta_s^0 \tilde{\eta}_s(\tilde{\Pi}). \tag{12}$$

Here, Π_ℓ is a typical pressure scale within the layer that will emerge from the momentum balance. Continuity (eq. 7) requires that the horizontal and vertical velocity scales be related as

$$V = \epsilon U. \tag{13}$$

The dimensionless momentum equations (6) become

$$\frac{\partial \tilde{\Pi}}{\partial \tilde{x}} = \tilde{\eta}_s \left(\frac{\partial^2 \tilde{u}}{\partial \tilde{y}^2} + \epsilon^2 \frac{\partial^2 \tilde{u}}{\partial \tilde{x}^2} \right) + 2\epsilon^2 \frac{\partial \tilde{\eta}_s}{\partial \tilde{\Pi}} \frac{\partial \tilde{\Pi}}{\partial \tilde{x}} \frac{\partial \tilde{u}}{\partial \tilde{x}} + \frac{\partial \tilde{\eta}_s}{\partial \tilde{\Pi}} \frac{\partial \tilde{\Pi}}{\partial \tilde{y}} \left(\frac{\partial \tilde{u}}{\partial \tilde{y}} + \epsilon^2 \frac{\partial \tilde{v}}{\partial \tilde{x}} \right), \tag{14}$$

and

$$\frac{\partial \tilde{\Pi}}{\partial \tilde{y}} = \epsilon^2 \tilde{\eta}_s \left(\frac{\partial^2 \tilde{v}}{\partial \tilde{y}^2} + \epsilon^2 \frac{\partial^2 \tilde{v}}{\partial \tilde{x}^2} \right) + 2\epsilon^2 \frac{\partial \tilde{\eta}_s}{\partial \tilde{\Pi}} \frac{\partial \tilde{\Pi}}{\partial \tilde{y}} \frac{\partial \tilde{v}}{\partial \tilde{y}} + \epsilon^2 \frac{\partial \tilde{\eta}_s}{\partial \tilde{\Pi}} \frac{\partial \tilde{\Pi}}{\partial \tilde{x}} \left(\frac{\partial \tilde{u}}{\partial \tilde{y}} + \epsilon^2 \frac{\partial \tilde{v}}{\partial \tilde{x}} \right), \tag{15}$$

whereupon

$$\Pi_\ell = \frac{\eta_s^0 U}{\epsilon h} \tag{16}$$

emerges as a natural surface pressure scale. We show in Appendix B that when

$$\epsilon \left| \frac{\partial \tilde{\eta}_s}{\partial \tilde{\Pi}} \right| \ll 1, \tag{17}$$

or equivalently when

$$\tau_{\max} = \left| \eta_s(\Pi) \frac{\partial u}{\partial y} \right|_{\max} \ll \Pi_c, \tag{18}$$

the (dimensional) lubrication equations for Π-dependent surface viscosities reduce to

$$\frac{\partial \Pi}{\partial x} = \eta_s(\Pi) \frac{\partial^2 u}{\partial y^2}, \tag{19}$$

$$\frac{\partial \Pi}{\partial y} = 0, \tag{20}$$

$$\frac{\partial u}{\partial x} + \frac{\partial v}{\partial y} = 0. \tag{21}$$

These equations are identical to their Newtonian 2D analogs, with the exception of the Π-dependence in η_s.

Within the thin film, $\eta_s(\Pi)$ is constant across the gap in the y-direction. Therefore, as with standard lubrication flows, a local flow solution can be obtained by integrating the x-momentum equation:

$$u(x, y) = \frac{1}{\eta_s(\Pi)} \frac{d\Pi}{dx} \left(\frac{y^2}{2} + By + A \right) \tag{22}$$

where A and B are constants determined by the boundary conditions at $y = 0$ and $y = h(x)$. Continuity can be enforced by imposing the relevant condition on the flux through the gap,

$$Q(x) = \frac{1}{\eta_s(\Pi)} \frac{d\Pi}{dx} \left(Ah(x) + \frac{Bh^2(x)}{2} + \frac{h^3(x)}{6} \right). \tag{23}$$

Generally, the flux is either specified (for a fixed geometry), or obeys some constraint (in the case of a moving body). For example, $Q(x) = Vx$ for two left-right symmetric surfaces that approach with a known velocity V, whereas $Q(x)$ must be constant or zero in flows through stationary geometries.

We first highlight a generic feature of Π-dependent surface viscosity by expressing Eq. (23) in the form

$$\frac{d\Pi}{dx} = \eta_s(\Pi)\ G(x), \tag{24}$$

where

$$G(x) = \frac{Q(x)}{Ah(x) + \frac{Bh^2(x)}{2} + \frac{h^3(x)}{6}} \tag{25}$$

is determined entirely by the system geometry and flow conditions. Eq. (24) is common to conventional lubrication analysis; if $\eta_s(\Pi)$ were constant, nothing new or surprising would occur.

Here, however, η_s generally has a strong, nonlinear dependence on Π, so that the ODE is fully nonlinear. Remarkably, however, this nonlinear ODE is separable, and thus can be written in the form

$$\frac{d\Pi}{\eta_s(\Pi)} = G(x)\ dx. \tag{26}$$

A formal solution may thus be obtained by directly integrating (26) for *any* functional form of $\eta_s(\Pi)$, whether taken from an empirical expression or directly from measurements, yielding

$$\int_{\Pi_0}^{\Pi} \frac{d\Pi'}{\eta_s(\Pi')} = \int_{x_0}^{x} G(x')\ dx'. \tag{27}$$

Here $\Pi_0 = \Pi(x_0)$ is a reference pressure, evaluated at x_0 (often taken to be far outside the gap):

We will express this solution as

$$q(\Pi) = g(x), \tag{28}$$

where

$$q(\Pi) = \int_{\Pi_0}^{\Pi} \frac{d\Pi'}{\eta_s(\Pi')}, \tag{29}$$

$$g(x) = \int_{x_0}^{x} G(x')\ dx'. \tag{30}$$

Remarkably, $g(x)$ depends only on the flow and geometry of the system, and is thus given by known solutions to Newtonian (constant-η) 2D lubrication problems. At the same time, $q(\Pi)$ depends only on the specific form of the Π-dependence of η_s, and can be integrated numerically from measured isotherms, or integrated directly for model expressions. The surface pressure distribution is thus found formally by inverting $q(\Pi)$, as expressed by

$$\Pi(x) = q^{-1}[g(x)]. \tag{31}$$

Π-dependent surface rheology naturally give rise to limiting velocities or fluxes, as can be easily seen by directly integrating (8) for pressure-thickening surfactants:

$$q(\Pi) = \frac{1}{\eta_s^0}\int_0^{\Pi} \frac{d\Pi'}{e^{\Pi'/\Pi_c}} = \frac{\Pi_c}{\eta_s^0}\left[1 - e^{-\Pi/\Pi_c}\right]. \tag{32}$$

Inverting $q(\Pi)$ gives

$$\Pi(x) = q^{-1}[g(x)] = -\Pi_c \log\left[1 - \frac{\eta_s^0}{\Pi_c} g(x)\right]. \tag{33}$$

whose logarithm diverges as its argument approaches zero. For real-valued solutions of $\Pi(x)$ to exist, only certain values are accessible to the function $g(x)$, which contains information about flow rate (*e.g.* for surface pressure-driven flow) or boundary velocity (when driven by relative motion between particles). This restriction on $g(x)$ therefore places upper bounds on the velocity or flow rate – a reflection of the increased resistance to flow with rising surface pressure.

We will explore three paradigmatic cases, each representing a different class of lubrication problems and illustrating an important process in surfactant dynamics: (1) pressure-driven flow through a stationary gap; (2) squeezing flow between two surfaces approaching each other; (3) standard lubrication problem of one surface moving relative to another.

III. PRESSURE-DRIVEN FLOW

The so-called 'surface-slit' [33] or 'canal surface' [34] viscometers were among the earliest methods to measure surface viscosity, and involve a narrow channel through which a surfactant monolayer is pushed by applying a surface pressure gradient [6, 31, 35–37]. These studies, however, assumed a constant surface viscosity and focused on quantifying the hydrodynamic coupling between the interface and the subphase. Here, we shall look at interfaces that are decoupled entirely from the subphase (Bo $\gg 1$), and highlight the qualitative effects of Π-dependent viscosity on surfactant flows through thin channels.

Specifically, we consider a surfactant monolayer flowing through a thin gap of constant width h between $x = 0$ and $x = L$, driven by a surface pressure imbalance far outside the gap (Fig. 2). The surface pressures at the ends of the channel are

$$\Pi(x = 0) = \Pi_0 + \Delta\Pi, \quad \Pi(x = L) = \Pi_0, \tag{34}$$

with $\Delta\Pi > 0$. The surfactant velocity profile within the channel is found by solving Eq. (19) and imposing no-slip boundary conditions at $y = 0$ and $y = h$ to determine the constants A and B, giving

$$u(x, y) = \frac{1}{2\eta_s(\Pi)} \frac{d\Pi}{dx} y(y - h), \tag{35}$$

$$Q = -\frac{h^3}{12\eta_s(\Pi)} \frac{d\Pi}{dx} = \text{constant}. \tag{36}$$

Note that these are the case-specific forms of the more general expression in Eqs. (22) and (23).

The Π-dependence of η_s results in a nonlinear ODE, but one which may be separated (as in Eq. (26)) as

$$\frac{d\Pi}{\eta_s(\Pi)} = -\frac{12Q}{h^3}\, dx. \tag{37}$$

Following eq. (30), the geometry- and flow-rate-dependence is contained within the function $g(x)$,

$$g(x) = -\int_L^x \frac{12Q}{h^3} dx = \frac{12Q}{h^3}(L - x). \tag{38}$$

Computing $q(\Pi)$ as in Eq. (29) requires a constitutive equation for $\eta_s(\Pi)$. For a Newtonian surfactant, $\eta_s(\Pi)$ is constant (η_s^0), for which $q(\Pi)$ becomes simply

$$q^N(\Pi) = \int_{\Pi_0}^{\Pi} \frac{d\Pi'}{\eta_s^0} = \frac{\Pi(x) - \Pi_0}{\eta_s^0}. \tag{39}$$

The pressure distribution in the channel follows by setting $q(\Pi) = g(x)$ as in Eq. (28), giving

$$\Pi(x) = \Pi_0 + \frac{12\eta_s^0 Q}{h^3}(L - x), \tag{40}$$

with the pressure decreasing linearly from $x = 0$ to $x = L$. Imposing Eq. (34) recovers the 2D analog of Poiseuille's law,

$$Q^N = \frac{\Delta\Pi}{L} \frac{h^3}{12\eta_s^0}. \tag{41}$$

A. Pressure-thickening

We now consider the most common surfactants, for which η_s thickens with surface pressure. We will assume $\eta_s^+(\Pi)$ increases exponentially with Π, (eq. 8), as is most common. In that case, $q(\Pi)$ in Eq. (29) is given by

$$q^+(\Pi) = \frac{\Pi_c}{\eta_s^0} \left(1 - e^{-(\Pi - \Pi_0)/\Pi_c}\right). \tag{42}$$

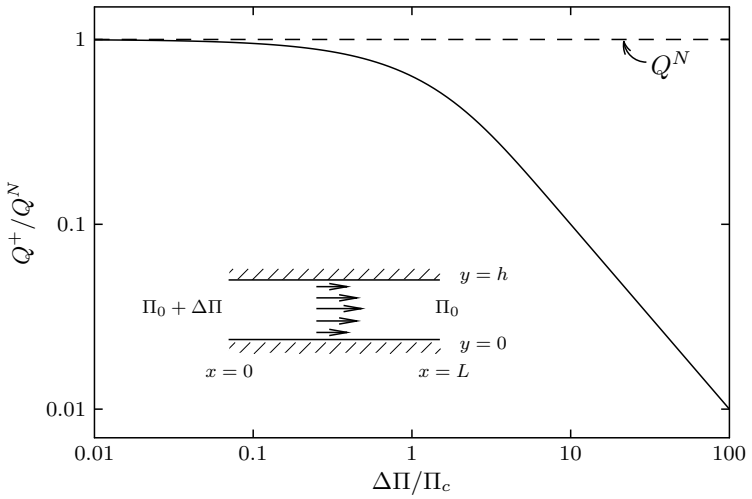

FIG. 2. Flux Q^+ of a Π-thickening surfactant driven through a channel, compared with its Newtonian analogue (Q^N). While Q^N increases linearly with the applied pressure difference $\Delta\Pi$, Q^+ approaches a constant when $\Delta\Pi \gtrsim \Pi_c$.

The flow- and geometry-dependent function $g(x)$ does not depend on surface rheology, and is therefore simply given by Eq. (38). The solution, then, is found by simply setting $q^+(\Pi) = g(x)$:

$$\frac{\Pi_c}{\eta_s^0}\left(1 - e^{-(\Pi-\Pi_0)/\Pi_c}\right) = \frac{12Q^+}{h^3}(L - x). \tag{43}$$

The flux of Π-thickening surfactant through a straight channel is then found by imposing (34) to give

$$Q^+ = \frac{\Pi_c}{L}\frac{h^3}{12\eta_s^0}\left(1 - e^{-\Delta\Pi/\Pi_c}\right) = Q^N\frac{\Pi_c}{\Delta\Pi}\left(1 - e^{-\Delta\Pi/\Pi_c}\right), \tag{44}$$

which is normalized by the Newtonian surfactant flux Q^N (Eq. (34)).

Fig. 2 shows the flux of Π-thickening surfactant as a function of applied surface pressure drop. The Newtonian limit, unsurprisingly, is recovered for small $\Delta\Pi/\Pi_c$:

$$Q^+(\Delta\Pi \ll \Pi_c) \approx Q^N\frac{\Pi_c}{\Delta\Pi}\left(1 - \left(1 - \frac{\Delta\Pi}{\Pi_c}\right)\right) \approx Q^N. \tag{45}$$

More dramatically, the surfactant flux is altered significantly when surface pressure differences become comparable to Π_c. In fact, the flux of Π-thickening surfactants approach a maximum, limiting value as $\Delta\Pi/\Pi_c \to \infty$:

$$Q^+(\Delta\Pi \gg \Pi_c) \to Q_{\max} = \frac{\Pi_c}{L}\frac{h^3}{12\eta_s^0}. \tag{46}$$

Effectively, the surface pressure scale Π_c sets the maximum pressure drop for the gradient. The origin of this non-intuitive result can be clarified by inverting Eq. (43) to obtain the surface pressure distribution

$$\Pi^+(x) = \Pi_0 - \Pi_c \ln\left[1 - \frac{12\eta_s^0 Q^+}{\Pi_c h^3}(L - x)\right] = \Pi_0 - \Pi_c \ln\left[1 - \frac{Q^+}{Q_{\max}}\left(1 - \frac{x}{L}\right)\right] \tag{47}$$

Since $Q^+ > 0$, there exists a maximum flux

$$Q_{\max} = \frac{\Pi_c h^3}{12\eta_s^0 L}, \tag{48}$$

beyond which the logarithm diverges within the channel (*i.e.* at some $x \leq L$).

The three-dimensional analog of Eq. (44) has been previously described in the context of 'choking' during the high-pressure processing of polymer melts [20, 21] using exponential $\eta - p$ relationships. Beyond recovering the surfactant

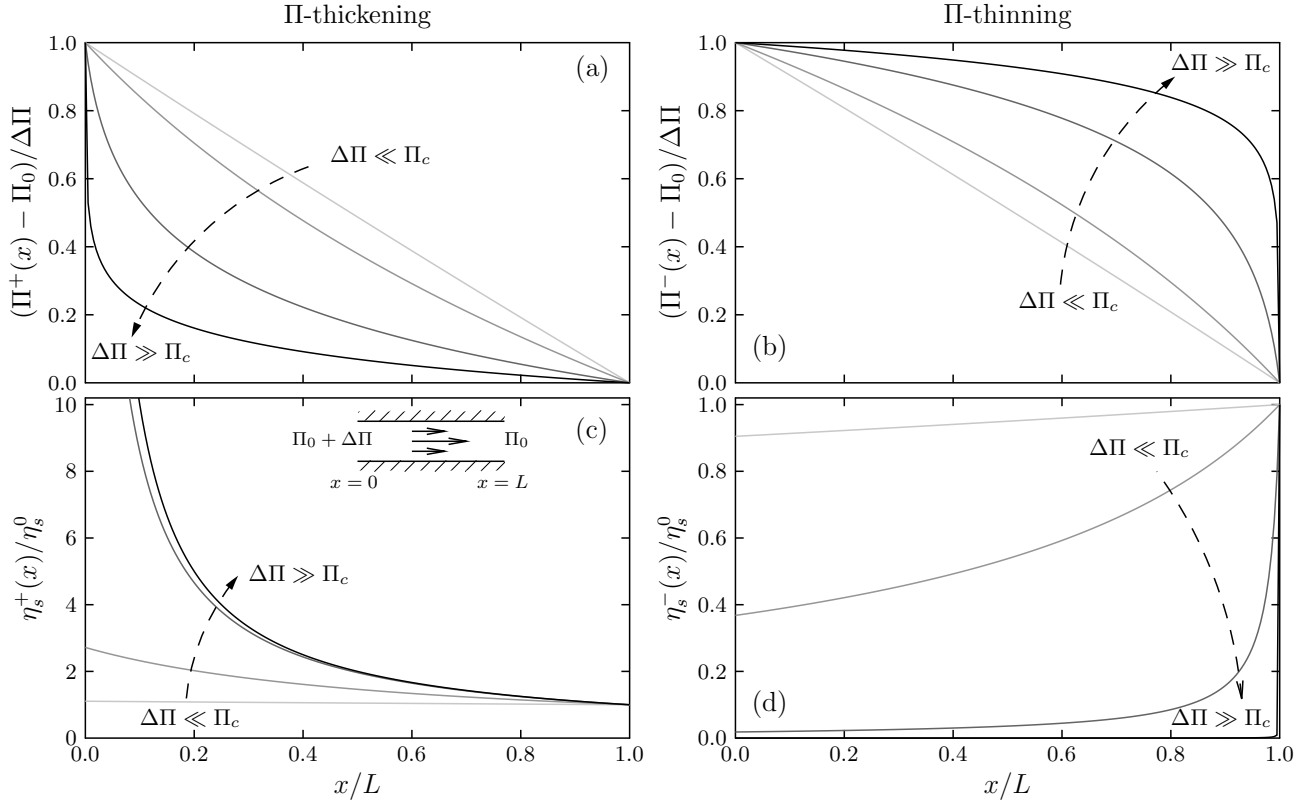

FIG. 3. Pressure and viscosity distributions in a channel for a Π-thickening ((a) and (c)) and a Π-thinning surfactant ((b) and (d)). The lines correspond to $\Delta\Pi/\Pi_c = 0.1$, 1, 4, and 10, with the dashed arrow indicating the direction of increasing $\Delta\Pi$ in each case.

analog of these previous studies, our analysis holds for channels of variable width $h(x)$, and for arbitrary $\eta_s(\Pi)$ relations. While an exponential form allows easy calculation, any general dependence can be integrated following Eq. (29), while maintaining the same geometry and flow conditions of Eq. (30).

The limiting flux can be understood physically as follows. The viscous resistance of a Newtonian surfactant to flow through a channel increases linearly with imposed surface pressure. When surface viscosity increases with surface pressure, the surfactant's viscous resistance grows more rapidly than linearly with surfactant flux, and is localized most strongly in regions where of highest surface pressure. When fluxes become large enough that $\Delta\Pi \gg \Pi_c$ would be required, the majority of the surface pressure gradient occurs along a short region near the entrance of the channel, where η_s is extremely high. Further increases to $\Delta\Pi$ largely change the viscosity within this thin region, and have little impact on the flux. Indeed, Π profile follows a linear (Newtonian) profile when $\Delta\Pi \ll \Pi_c$, because η_s does not change appreciably under those conditions, but becomes highly skewed for large $\Delta\Pi/\Pi_c$ (Fig. 3a). In the latter case, the pressure profile near $x = L$ has an approximate slope given by Π_c/L, as dictated by the maximum flux. An upstream boundary layer corrects this close to $x = 0$, where the viscosity is highest (Fig. 3(c)). The result is that the local pressure remains of the order of Π_c for a majority of the channel regardless of the applied pressure difference $\Delta\Pi$, therefore setting an upper bound on the flux that can be pumped through it.

Such a self-limiting nature of the flux can have unexpected implications in situations where surfactants are forced through narrow channels. For instance, fluid compressibility gives rise to anomalously long transients in response to steady pressurization along microfluidic channels (the 'bottleneck' effect) [38]. Related phenomena have been observed in surfactant monolayers as well, owing either to non-uniform surface viscosity [37], or the 2D bottleneck effect [39], or perhaps some combination. For example, DPPC ($\eta_s^0 \sim 10\,\mu$Ns/m), driven with mm/s velocities through a narrow slit of width $h = 0.5$ mm and length $L = 5$ mm would require surface pressure difference $\Delta\Pi \gtrsim \Pi_c \sim 8\,$mN/m, where departures from Newtonian behavior may be expected. Albeit derived for a simple constitutive relation between η_s and Π, our analysis indicates a highly non-linear dependence of flow rate on the applied pressure difference – analogous to choking in (3D) polymer processing [21].

B. Pressure-thinning

Repeating the analysis for pressure-thinning surfactants, where $\eta_s(\Pi)$ now decreases with Π according to (9) gives

$$q^-(\Pi) = \frac{\Pi_c}{\eta_s^0}\left(e^{(\Pi-\Pi_0)/\Pi_c} - 1\right). \tag{49}$$

The pressure distribution in the channel is found by setting $q^-(\Pi) = g(x)$, giving

$$\Pi^-(x) = \Pi_0 + \Pi_c \ln\left[1 + \frac{12\eta_s^0 Q^-(L-x)}{h^3\Pi_c}\right] \tag{50}$$

to result in a pressure-thinning surfactant flux

$$Q^- = \frac{\Pi_c}{L}\frac{h^3}{12\eta_s^0}\left(e^{\Delta\Pi/\Pi_c} - 1\right) = Q^N\frac{\Pi_c}{\Delta\Pi}\left(e^{\Delta\Pi/\Pi_c} - 1\right). \tag{51}$$

The linear (Newtonian) flux is recovered for $\Delta\Pi \ll \Pi_c$, as expected and can verified by Taylor expansion. When $\Delta\Pi \gg \Pi_c$, on the other hand, the flux grows exponentially with applied surface pressure. In this case, increasing pressure decreases viscosity, reducing viscous resistance over an increasing fraction of the channel. Pressure-thinning permits the surface pressure to remain of the order of the driving pressure $\Delta\Pi$ for the majority of the channel (Fig. 3b), with a boundary layer now at the downstream end (where the viscosity is highest) across which the pressure drops to $\Pi(x = L) = \Pi_0$. Surface viscosity is significantly reduced for the majority of the channel (Fig. 3d), offering reduced resistance to flow and allowing the flux to increase without bound as $\Delta\Pi$ increases.

IV. BOUNDARY-DRIVEN FLOW

We move on now to a set of classical lubrication problems – that of flow in thin gaps driven by the relative motion of the confining boundaries. The width of the fluid gap is assumed to be much smaller than the linear dimension of the particles that confine the flow to the gap, so that the approximations of lubrication theory hold. These examples, besides being within the reach of established experimental techniques [8, 12], will also serve as building blocks towards developing the physical intuition and the mathematical machinery behind suspension-level interactions. We shall consider two representative cases, both involving two surfaces separated by a thin gap and approaching each other or sliding past one another. Specific examples include a circular disk approaching a wall, and a two-dimensional journal bearing, respectively.

A. Disk approaching a wall

We now consider a circular disk of radius R moving at a constant velocity V towards a stationary wall at $y = 0$, separated by a gap $h(x)$. When the gap width h_0 is much smaller than R, the gap profile is given approximately by

$$h(x) = h_0(1 + x^2/L_{\text{circ}}^2), \tag{52}$$

where

$$L_{\text{circ}} = \sqrt{2h_0R}. \tag{53}$$

In the Bo$\gg 1$ (interfacially-dominated) limit of interest here, we will assume that the thickness of the disk and the subphase drag are both negligible. Following eq. (22) and imposing no-slip conditions, the fluid velocity and local flux are given by

$$u(x,y) = \frac{1}{2\eta_s(\Pi)}\frac{d\Pi}{dx}y(y - h(x)), \tag{54}$$

$$Q = -\frac{1}{12\eta_s(\Pi)}\frac{d\Pi}{dx}h^3(x). \tag{55}$$

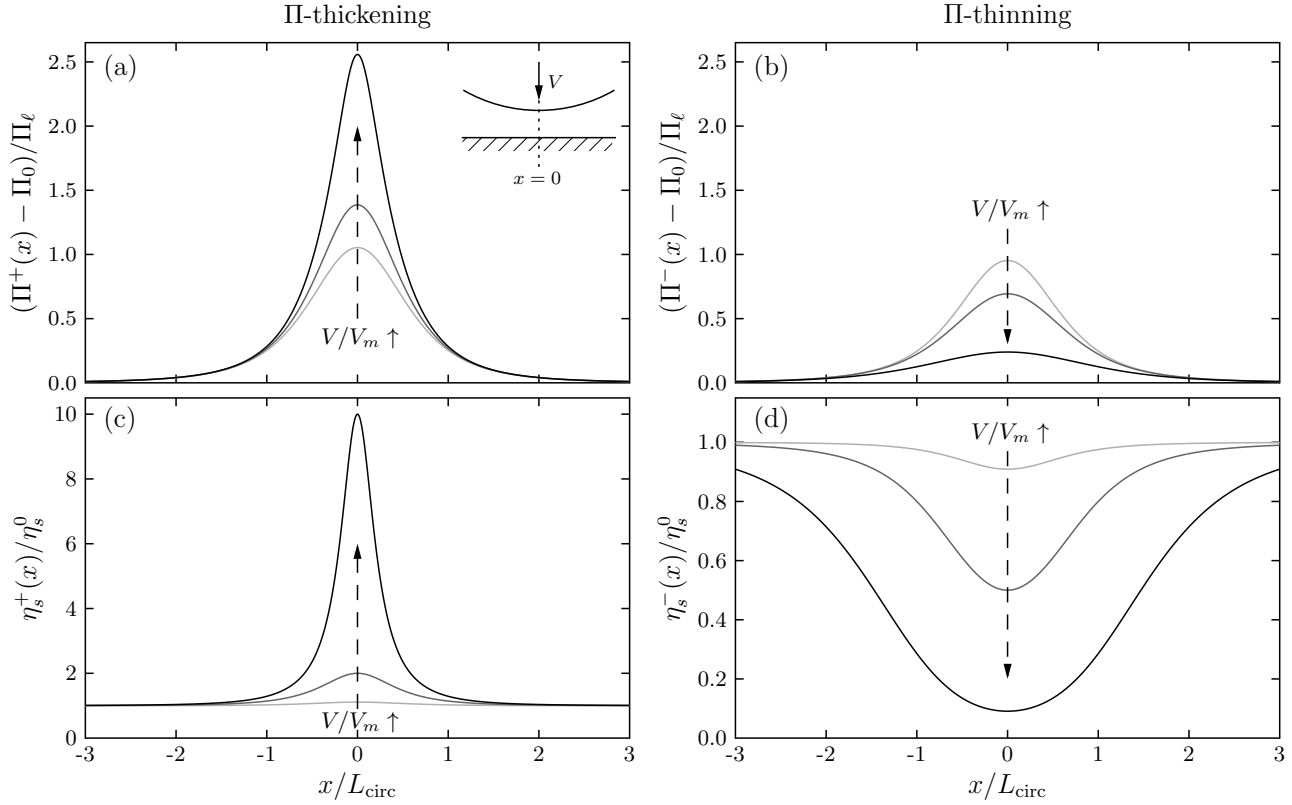

FIG. 4. Pressure and viscosity distributions in the gap between an approaching disk and a wall for a Π-thickening ((a) and (c)) and a Π-thinning surfactant ((b) and (d)). In the Π-thickening case, the approach velocity can not exceed a maximum value $V = V_m$, with V/V_m =0.1, 0.5, and 0.9 depicted. No maximum approach velocity exists for Π-thinning surfactants. Lines correpsond to V/V_m =0.1, 1, and 10.

As with standard lubrication problems, we assume the surface pressure to approach a 'far-field' pressure $\Pi_0 = \Pi(\pm\infty)$ before the approximation $h(x)$ for the film thickness breaks down. Given the left-right symmetry of the system, mass conservation specifies the squeeze flux through the gap to obey

$$Q = Vx, \tag{56}$$

which gives an ODE,

$$\frac{d\Pi}{\eta_s(\Pi)} = -\frac{12Vx}{h(x)^3}dx, \tag{57}$$

here written in separable form.

We will work again with the definitions of the flow- and geometry-dependent and viscosity-dependent functions $q(\Pi)$ and $g(x)$ from Eqs. (29) and (30), giving

$$g(x) = -\frac{12V}{h_0^3}\int_{-\infty}^{x}\frac{x'}{(1+x'^2/L_{\rm circ}^2)^3}dx' = \frac{3VL_{\rm circ}^2}{h_0^3}\frac{1}{(1+x^2/L_{\rm circ}^2)^2}. \tag{58}$$

The function $q(\Pi)$ depends on the specific surfactant. For a Newtonian surfactant with constant η_s^0, $q^N(\Pi)$ is given by (39), giving a surface pressure profile

$$\Pi^N(x) = \Pi_0 + \frac{\Pi_\ell}{(1+x^2/L_{\rm circ}^2)^2}, \tag{59}$$

where we have defined

$$\Pi_\ell = \Pi^N(x=0) = \frac{3V\eta_s^0 L_{\rm circ}^2}{h_0^3} \tag{60}$$

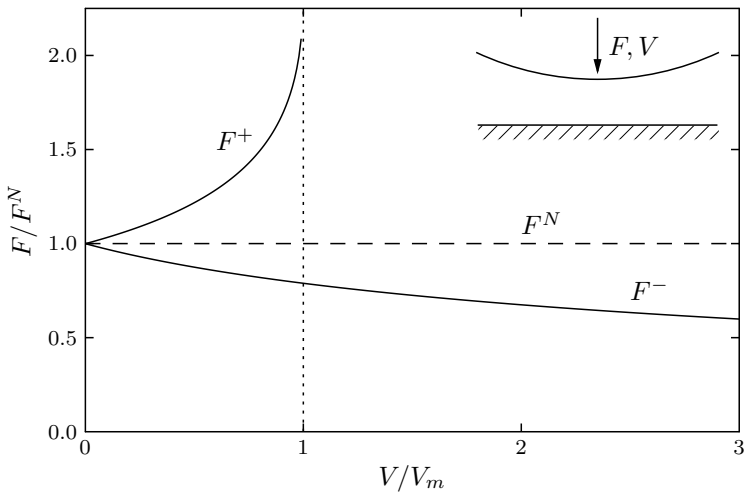

FIG. 5. Force-velocity relations for a circular disk approaching a wall in Π-thickening and Π-thinning mediums. The vertical dotted line represents the maximum velocity of approach in a Π-thickening surfactant, at which point the force diverges.

as a reference surface pressure scale within the thin gap.

Surface pressure-thickening and -thinning surfactants, whose surface viscosity $\eta_s^{\pm}(\Pi)$ follow Eqs. (8) and (9) and have $q^{\pm}(\Pi)$ given by (42) and (49). Inverting $q^{\pm}(\Pi) = g(x)$, yields surface pressure distributions

$$\Pi^{+}(x) = \Pi_0 - \Pi_c \ln\left[1 - \frac{\Pi_\ell}{\Pi_c}\frac{1}{(1+x^2/L_{\rm circ}^2)^2}\right], \tag{61}$$

$$\Pi^{-}(x) = \Pi_0 + \Pi_c \ln\left[1 + \frac{\Pi_\ell}{\Pi_c}\frac{1}{(1+x^2/L_{\rm circ}^2)^2}\right], \tag{62}$$

In both cases, the Newtonian distribution (59) is recovered in the large-Π_c limit: $\Pi^N(x) \approx \Pi^{\pm}(x, \Pi_c \to \infty)$.

A maximum approach velocity exists for disks approaching a wall in pressure-thickening monolayers, analogous to the limiting flux in channel flows. Likewise, a maximum separation velocity exists for disks moving away from a wall in pressure-thinning monolayers. The pressure distribution described by Eq. (61) is non-singular only when $\Pi_\ell \le \Pi_c$, defining a maximum approach (separation) velocity in Π-thickening (thinning) surfactants:

$$V \le V_m = \frac{\Pi_c h_0^3}{3\eta_s^0 L_{\rm circ}^2}. \tag{63}$$

The velocity maximum has a simple physical explanation. The large lubrication pressures in the gap grow with with η_s, which in turn increases with Π in a pressure-thickening surfactant. Increasing the approach velocity increases Π, which increases $\eta_s(\Pi)$, which requires a larger Π, and so on. Ultimately, V_m is a critical approach velocity at which the resistance to motion diverges. Surfactants behave as Newtonian when $V \ll V_m$, but behave differently as $V \sim V_m$. Such qualitatively distinct dynamics should be experimentally accessible: microfabricated, ferromagnetic micro-button probes [11] ($R \sim 50\,\mu$m) separated $h_0 \sim 10\,\mu$m from a wall in DPPC ($\Pi_c \sim 8\,$mN/m, and $\eta_s^0 \sim 10\,\mu$Ns/m), would exhibit a maximum velocity $V_m \sim 10\,\mu$m/s; .

Because $V/V_m = \Pi_\ell/\Pi_c$, the surface pressure profiles may be expressed in terms of the approach velocity as

$$\frac{\Pi^{\pm}(x) - \Pi_0}{\Pi_\ell} = \mp\frac{V_m}{V}\ln\left[1 \mp \frac{V}{V_m}\frac{1}{(1+x^2/L_{\rm circ}^2)^2}\right]. \tag{64}$$

Figure 4 shows $\Pi^{\pm}(x)$ for Π-thickening and -thinning interfaces. The increasing pressure in the thin film changes the viscosity locally and this in turn increases (or decreases) the pressure in a Π-thickening (or thinning) system relative to a Newtonian fluid, with the effect accentuated with increasing approach velocity V. The corresponding viscosity distribution (Figure 4(c)) peaks at $x = 0$ and becomes singular as $V \to V_m$ for a Π-thickening surfactant. In a Π-thinning surfactant, however, there is no such upper bound on the approach velocity. Instead, the local surface pressure grows increases like $\Pi^- \sim \Pi_c \ln(V/V_m)$ for large velocities, *i.e.* much more slowly than the Newtonian $\Pi^N \sim V$. Consequently, a low viscosity is maintained in the gap (Figure 4(d)), and the surfactant may be squeezed out of the gap more easily.

With the pressure distribution in the gap now known, we may calculate the force required to drive the particle towards the wall at a given velocity by integrating the stress on the particle surface in contact with the thin film. The predominant contribution of the stress in the lubrication layer is due to the pressure, and owing to the slow change in cross-section of the lubrication layer, the net force F acting on the particle is approximately the integral of $\Pi(x)$ across x. In a Newtonian lubrication layer, the force is linear in the approach velocity: $F^N \sim V$. Upon inspecting $\Pi^{\pm}(x)$, we note that a significant pressure difference occurs only around $x = 0$ (see Fig. 4(a)-(b)), and a coarse approximation to the integral is $F^{\pm} \sim \mp \ln(1 \mp V/V_m)$. In particular, this predicts that the force acting on a circular disk in a pressure-thinning monolayer grows approximately as $F^- \sim \ln(V)$ when $V \gg V_m$. A Π-thinning surfactant becomes easier to squeeze out from the gap, with the approach velocity growing exponentially with squeezing force: $V \sim V_m e^F$.

In a Π-thickening monolayers, by contrast, the force *diverges* near the maximum approach velocity: $F^+ \sim -\ln(1 - V/V_m)$. The surface pressure and surface viscosity also diverge as $V \to V_m$ (Fig. 4). Physically, the surfactant within the thin gap becomes increasingly harder to squeeze out. Even with an arbitrarily large squeezing force, the disk approaches at a finite velocity $V \sim V_m(1 - e^{-F})$. The numerically integrated force-velocity relations for all cases are shown in Fig. 5.

The departure from Newtonian behavior can be further elucidated for small velocities. Expanding the pressure distributions from Eq. (64) in a Taylor series in V/V_m, and integrating across x, the force retarding the disk's motion is

$$\frac{F^{\pm}}{\Pi_\ell L_{\rm circ}} = \frac{1}{L_{\rm circ}} \int_{-\infty}^{\infty} \frac{\Pi^{\pm}(x) - \Pi_0}{\Pi_\ell}\, dx = \frac{\pi}{2} \pm \frac{5\pi}{32} \frac{V}{V_m} + \mathcal{O}\left(\left(\frac{V}{V_m} \right)^2 \right), \tag{65}$$

where the first term recovers the Newtonian result (59), with $F^N = \pi \Pi_\ell L_{\rm circ}/2$. The leading effect of Π-dependent surface rheology, when $V \ll V_m$, is to increase (when Π-thickening) or decrease (when Π-thinning) the net vertical force on the body, consistent with the pressure distributions in Fig. 4(a)-(b) and the force-velocity relations in Fig. 5.

B. Journal bearing

We finally turn to the surfactant analog of the journal bearing problem, whose geometry is significantly more complicated than our previous examples. While this geometry has been studied numerically for piezo-viscous fluids [22], this example highlights the ease with which Newtonian results may be adapted to surfactant-laden interfaces with arbitrary $\eta_s(\Pi)$ relations. The 2D analogue of the journal bearing (Fig. 6) consists of an inner cylinder of radius a rotating at angular velocity Ω within a stationary cylindrical cavity of radius b, with the void in between being filled with a surfactant. The centers of the two circles are separated by a distance c. We shall define the clearance ϵ and eccentricity λ, both dimensionless, such that $b = a(1 + \epsilon)$, and $c = \lambda a \epsilon$. Concentric circles correspond to $\lambda = 0$, whereas circles touch when $\lambda = 1$. We define the origin to be centered at the inner circle, with $x = 0$ along the line connecting the centers, and θ measuring the angle winding from the maximum gap thickness at $\theta = 0$. To leading order in ϵ, the gap profile is $h(\theta) = a\epsilon(1 + \lambda \cos\theta)$. Newtonian results are readily available (*e.g.* [40]), and can be adated for Π-dependent η_s, according to

$$\frac{d\Pi}{d\theta} = -\frac{6\eta_s(\Pi)\Omega}{\epsilon^2(2 + \lambda^2)} \left[\frac{3\lambda^2 + (2 + \lambda^2)\lambda \cos\theta}{(1 + \lambda \cos\theta)^3} \right]. \tag{66}$$

In a Newtonian fluid with constant η_s^0, and the pressure distribution follows from direct integration, giving

$$\Pi^N(\theta) = -\frac{6\eta_s^0 \Omega}{\epsilon^2} \Lambda(\lambda, \theta), \tag{67}$$

where

$$\Lambda(\lambda, \theta) = \left[\frac{\lambda \sin\theta (2 + \lambda \cos\theta)}{(2 + \lambda^2)(1 + \lambda \cos\theta)^2} \right]. \tag{68}$$

We have set the the reference pressure $\Pi(\theta = 0)$ to zero without loss of generality, owing to the periodicity in θ. The Newtonian distribution appears as the dashed line in Fig. 7(a), showing an important symmetry in the Newtonian system, a consequence of which is that there is zero net radial force on the inner cylinder (the 'journal'). The lack of a transverse force also holds for a cylinder sliding next to a wall in Newtonian Stokes flows. In fact, the kinematic reversibility of Stokes flows [40] forbits any net hydrodynamic force perpendicular to the wall. Surfactants with $\Pi-$dependent rheology break this symmetry, a point we shall return to shortly.

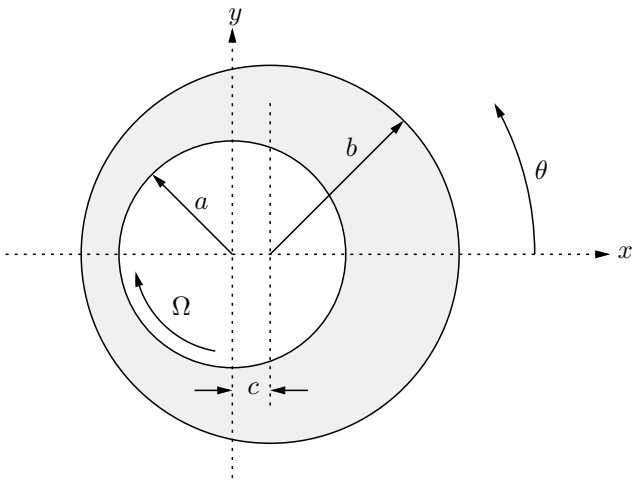

FIG. 6. Geometry of the journal bearing.

When the gap is filled with a surfactant with Π−dependent surface viscosity $\eta_s(\Pi)$, however, will break this symmetry and give rise to qualitatively distinct effects. Eq. (66) can be separated following the approach described throughout this work. The flow- and geometry-dependent integral, $g(x)$, is identical to the corresponding Newtonian problem (67), which we can adopt directly and separate to give

$$\int_0^{\Pi} \frac{d\Pi'}{\eta_s(\Pi')} = -\frac{6\Omega}{\epsilon^2}\Lambda(\lambda,\theta). \tag{69}$$

Note the ease with which a known Newtonian lubrication solution can be imported into the current framework. Using $q^{\pm}$ for exponentially pressure-thickening (or thinning) surfactants (eqs. 42 and 49) gives surface pressure profiles

$$\Pi^{\pm}(\theta) = \mp\Pi_c \ln\left[1 \pm \frac{6\eta_s^0\Omega}{\epsilon^2\Pi_c}\Lambda(\lambda,\theta)\right]. \tag{70}$$

Λ is odd-symmetric about $\theta = \pi$, and hence, the logarithmic dependence of $\Pi(\theta)$ on Λ sets a critical angular velocity in both Π-thickening and -thinning surfactants. This is expected, given that an increase in pressure on one side of the inner cylinder is simultaneously met with a decrease in pressure on the other side, and *vice versa*, within the lubrication domain.

A characteristic pressure scale for the Newtonian fluid is

$$\Pi_\ell = \Pi^N(\theta = \theta_m), \tag{71}$$

where θ_m is the angle of the maximum lubrication pressure,

$$\cos\theta_m = -3\lambda/(2+\lambda^2). \tag{72}$$

Fig. 7(a) shows $\Pi^{\pm}(\theta)$ normalized by Π_ℓ for pressure-thickening surfactant. The odd-symmetry of the pressure profile about $\theta = \pi$ in a Newtonian fluid is broken when the viscosity depends on surface pressure. The surface pressure distribution for a Π-thinning surfactant is found by simply reversing the features in the second and third quadrants. In both cases, solutions exist only for angular velocities below a critical value Ω_m, which depend on Π_c and the geometric factors λ and ϵ:

$$\Omega_m = \frac{\Pi_c\epsilon^2}{6\eta_s^0\Lambda(\lambda,\theta_m)}. \tag{73}$$

The net force on the inner cylinder is

$$\{F_x, F_y\} = -\int_0^{2\pi} \Pi(\theta)\, a\{\cos\theta, \sin\theta\}\, d\theta, \tag{74}$$

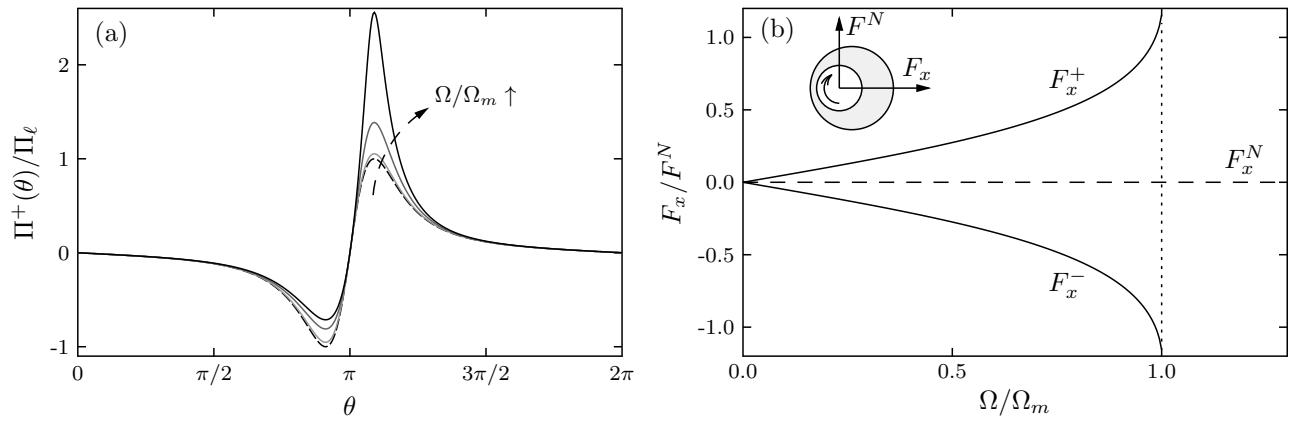

FIG. 7. (a) Pressure distribution in a Π-thickening surfactant in a 2D journal bearing. For the sake of illustration, we choose $\lambda = c/(b-a) = 0.9$ in this case. The arrow points to the direction of increasing angular velocity, with $\Omega/\Omega_m = 0.1$, 0.5, and 0.9. The dashed line is the Newtonian pressure distribution $\Pi^N(\theta)$. (b) Radial (or horizontal, in the geometry of Fig. 6) force on the inner cylinder. For a Newtonian fluid, $F^N = F_y^N$ and $F_x^N = 0$.

which can be evaluated numerically. Owing to kinematic reversibility in Stokes flow, the inner cylinder experiences zero net force along the line connecting the centers of cylinders when the lubricating fluid is Newtonian, and the Newtonian lubrication force F^N is exclusively in the y direction [40]. Fig. 7(b) shows the qualitative differences for Π-dependent surface viscosities. Solutions cease to exist beyond the critical angular velocity Ω_m, which corresponds to a diverging force on the inner cylinder. When $\Omega < \Omega_m$, the lubrication force perpendicular to the line of centers (F_y) is identical for both pressure-thickening and -thinning surfactants. This is linked to the fact that pressure-thickening on one side of the cylinder is matched by thinning on the other – a decrease in the resistance to push fluid out of the way is matched by an increase in resistance to draw fluid on the other side.

More interesting is the non-zero horizontal force F_x for both Π-thickening and Π-thinning surfactants. The fore-aft asymmetry in the pressure profile creates a 'lift' force that pushes (or pulls) the inner cylinder away from (or towards) the outer cylinder, depending on the surfactant. F_x diverges as $\Omega \to \Omega_m$, with Π-thickening and Π-thinning monolayers exhibiting lateral forces F_x that are equal in magnitude but opposite in sign: Lubrication forces in Π-thickening surfactants push the journal towards the center of the outer cylinder, whereas those in Π-thinning surfactants force the journal towards the wall of the outer cylinder.

Insight into the nature of the lubrication forces can be gained by examining the force analytically for small angular velocities. Taylor expanding $\Pi(\theta)$ in a Taylor series in Ω/Ω_m to order $(\Omega/\Omega_m)^3$, reveals

$$F_y^{\pm} \sim \frac{12\pi\eta_s^0\Omega a}{\epsilon^2}\left[\frac{\lambda}{(2+\lambda^2)(1-\lambda^2)^{1/2}}\right], \tag{75}$$

$$F_x^{\pm} \sim \pm\frac{18\pi(\eta_s^0\Omega)^2 a}{\epsilon^4\Pi_c}\left[\frac{\lambda^3(3-2\lambda^2)}{(2+\lambda^2)^2(1-\lambda^2)^{5/2}}\right]. \tag{76}$$

Both functions within square brackets above are positive, since $\lambda \in [0,1]$. To leading order, F_y is identical to the Newtonian lubrication force F^N obtained by integrating Eq. (67), irrespective of Π-thinning or thickening. The first effect of Π-dependent rheology appears in the radial force F_x acting along the line of centers, where quadratic dependence on Ω gives rise to a symmetry-breaking.

Physically, in a Π-thickening surfactant, this force acts to push the inner cylinder towards the center of the outer cylinder, and conversely pulls it closer to the edge in a Π-thinning surfactant. This lateral force introduces a qualitatively distinct response, which may be readily observed experimentally by rotating a force-free inner cylinder at constant angular velocity. In a Newtonian fluid or Newtonian surfactant, the inner disk would orbit the center of the outer cylinder, but maintain the same eccentricity. A Π-thickening surfactant would constantly generate a force on the inner cylinder towards the center of the outer cylinder, causing the inner cylinder to reduce the eccentricity over long times as it spirals towards the stable fixed point at the center. The opposite should occur with Π-thinning surfactants: this radial force is directed outward, driving the cylinder to spiral outward with ever-increasing eccentricity, with a radial force that increases with time. Moreover, this loss of kinematic reversibility can be realized in the simpler case of a disk translating next to a straight wall – the same physical reasons dictate that such a disk would experience a net force away from or towards the wall when the surrounding fluid is a surfactant with Π-dependent surface rheology, breaking the symmetries of Stokes flow.

V. IMPLICATIONS AND CONCLUSIONS

We have focused on the consequences of a surface rheological characteristic that is common to almost all insoluble surfactant monolayers – that of surface-pressure-dependent viscosity. For analytical tractability, we restricted our attention to the high-Boussinesq limit where viscous stresses from the bulk are subdominant, and we assumed negligible compressibility. We worked with lubrication geometries, where large surface pressure gradients arise naturally, and therefore accentuate effects of Π-dependent surface rheology. In addition to experimental accessibility, thin gap lubrication geometries are advantageous because the classical results of 2D lubrication can be adapted directly to systems with Π-dependent surface viscosity, for an arbitrary form of $\eta_s(\Pi)$.

The surface-pressure-dependence of viscosity manifests in non-intuitive ways in thin gap flows, characterized by self-limiting behavior and irreversible dynamics otherwise absent in these systems. In two-dimensional channel flows, the flux of a Π-thickening surfactant was shown to saturate at a maximal value, no matter how large the surface pressure gradient. This has implications in measurements performed in thin channels, where the '2D bottleneck effect' suggests that transport phenomena might be occurring at a far slower pace than expected. In the same vein, our analysis suggests guidelines for the selection of surfactants if such a limiting flux is indeed desired in a channel flow, based on the appropriate pressure scale Π_c. When two bodies approach each other or slide past one another in a Π-thickening surfactant, there exists a critical maximum velocity of translation (or rotation) beyond which the force required to move the body diverges. We qualitatively illustrated the physical reasoning behind kinematic irreversibility in such interactions.

More broadly, lubrication interactions comprise an important limit in suspension dynamics. The examples treated here suggest that Π-dependent surface rheology may profoundly impact the microstructure and dynamics of suspensions of 2D inclusions within surfactant-laden interfaces. For instance, a pair of particles approaching each other in a Π-thinning surfactant sets up large lubrication stresses in the gap between them, thereby decreasing the viscosity, and hence enabling their more rapid approach. Two such particles forced to separate, by contrast, would do so more slowly for the same reasons. The converse holds for Π-thickening surfactants: particles should approach slowly, but separate rapidly. The microstructural arrangement of particles will thus be anisotropic: particle pairs would behave differently in the compressional and extensional sides of an imposed flow [41], accentuated to different degrees in different quadrants in Π-thinning or Π-thickening surfactants. Analogous irreversibility in particle trajectories and the associated suspension microstructure have been reported in bulk fluid suspensions due to shear-thinning in the continuous fluid [42]. We leave these problems for future work, but expect the intuition and qualitative ideas presented here to inform these problems.

For completeness, we mention several physical effects that we have neglected, that could play significant roles in systems with Π-dependent rheology. We neglected surfactant compressibility, but could incorporate it explicitly by tracking the surfactant concentration field in a mass conservation equation. This could be further generalized by accounting for the kinetics of adsorption and desorption of species to and from the bulk, in the case of soluble surfactants [43] and nanoparticles [44–46]. Surface dilatational viscosities, which would generally also be Π-dependent, may also play a significant role in flows with a compressional contribution. Notably, however, high dilatational viscosities act to retard surfactant compression (or dilation), thereby rendering our 'quasi-Boussinesq' approximation more accurate.

VI. ACKNOWLEDGEMENTS

We acknowledge the National Science Foundation (NSF) under Grant CBET-1512833 for primary support of this work.

Appendix A: Interfacial momentum equation

We discuss here the relative importance of the various terms in the governing equations, and their reduction to the forms in Eqs. (6 – 7). Non-dimensionalizing the interfacial momentum equation by scaling velocities over a characteristic value U_0, lengths over L, and surface pressure over $\eta_s^0 U_0/L$ yields

$$\tilde{\boldsymbol{\nabla}}_s\tilde{\Pi} = \tilde{\boldsymbol{\nabla}}_s\cdot(\tilde{\eta}_s(\tilde{\boldsymbol{\nabla}}\tilde{\mathbf{u}}_s + \tilde{\boldsymbol{\nabla}}\tilde{\mathbf{u}}_s^T)) + \tilde{\boldsymbol{\nabla}}_s\left[\left(\frac{\kappa_s^0}{\eta_s^0}\tilde{\kappa}_s - \tilde{\eta}_s\right)\tilde{\boldsymbol{\nabla}}_s\cdot\tilde{\mathbf{u}}_s\right] + \frac{1}{\mathrm{Bo}}\left.\frac{\partial\tilde{\mathbf{u}}}{\partial\tilde{z}}\right|_{\tilde{z}=0}. \tag{A1}$$

Recognizing that the magnitude and Π-dependence of the two surface viscosities may be different, we scale each separately,

$$\eta_s(\Pi) = \eta_s^0 \tilde{\eta}_s(\tilde{\Pi}) \tag{A2}$$

and

$$\kappa_s(\Pi) = \kappa_s^0 \tilde{\kappa}_s(\tilde{\Pi}), \tag{A3}$$

where η_s^0 and κ_s^0 are characteristic values.

Surfactant concentration gradients correspond to surface pressure gradients, and the compressibility of the surfactant layer is described by the Gibbs elasticity of the interface,

$$E = \Gamma \frac{\partial \Pi}{\partial \Gamma}, \tag{A4}$$

so that small relative changes in concentration and surface pressure are connected according to

$$\frac{\Delta\Gamma}{\Gamma} = \frac{\Delta\Pi}{E}. \tag{A5}$$

The Gibbs elasticity therefore sets a scale for surface pressure variations required to drive significant changes in surfactant concentration. Specifically, if $\Delta\Pi \ll E$, only very small relative changes surfactant concentration arise. Most theoretical studies thus far (*e.g.* on a probe forced to translate within a monolayer [35, 47, 48]) assume interfaces to behave as 2D incompressible fluids.

Relative incompressibility, as expressed by small surface velocity divergence, is not alone sufficient to justify the neglect of surface dilatational viscous stresses in the momentum equation relative to surface shear stresses. Dilatational stresses are generated by changes in surface species concentration Γ, which obeys a conservation equation, *e.g.*,

$$\frac{\partial \Gamma}{\partial t} = -\boldsymbol{\nabla}_s \cdot (\Gamma \mathbf{u}_s), \tag{A6}$$

which in this case we have assumed to be advection-dominated. This equation can be reformulated using the Gibbs elasticity (Eq. (A4)) to give

$$\boldsymbol{\nabla}_s \cdot \mathbf{u}_s = -\frac{1}{\Gamma}\frac{D\Gamma}{Dt} = -\frac{1}{E}\frac{D\Pi}{Dt}, \tag{A7}$$

with dimensionless form

$$\tilde{\boldsymbol{\nabla}}_s \cdot \tilde{\mathbf{u}}_s = -\frac{\eta_s^0 U_0}{EL}\frac{D\tilde{\Pi}}{D\tilde{t}}. \tag{A8}$$

When the assumed surface pressure scale $\Delta\Pi \sim \eta_s^0 U_0/L$ is small compared with the Gibbs elasticity E, effects of surfactant compressibility maybe safely neglected.

Introducing Eq. (A7) into the momentum equation (A1) gives

$$\tilde{\boldsymbol{\nabla}}_s \left[\left(1 + \left(\frac{\kappa_s^0 U_0}{EL}\tilde{\kappa}_s - \frac{\eta_s^0 U_0}{EL}\tilde{\eta}_s \right) \frac{D}{D\tilde{t}} \right) \tilde{\Pi} \right] = \tilde{\boldsymbol{\nabla}}_s \cdot (\tilde{\eta}_s (\tilde{\boldsymbol{\nabla}}\tilde{\mathbf{u}}_s + \tilde{\boldsymbol{\nabla}}\tilde{\mathbf{u}}_s^T)). \tag{A9}$$

This form of the surface stress equation highlights conditions under which compression is significant. Specifically, the stresses associated with surface-divergent velocity fields have the form

$$\frac{\text{Surface stress}}{\text{Gibbs elasticity}}\frac{D\tilde{\Pi}}{D\tilde{t}}, \tag{A10}$$

highlighting the possibility that the dynamic contribution of surface pressure gradients may balance viscous shear stresses. In compressing surfactant interfaces, then, surface dilatation may play a significant role when the relative magnitude of the surface dilatational viscous stress, $\Pi_d = \kappa_s^0 U_0/L$, which arise due to temporal changes to surface pressure, exceeds the Gibbs elasticity. When $U_0 \ll EL/\kappa_s^0$, particle motions in the interface have low enough velocities that local surfactant concentrations change slowly enough that surface dilatational stresses are negligible. When $\Pi_d \ll E$, surface dilatational viscous stresses may be safely ignored and interfaces may be treated as effectively incompressible. The incompressible Boussinesq-Scriven equations (6 – 7) then follow naturally.

Appendix B: Lubrication scaling

The validity and limitations of the lubrication equations within the thin gap are detailed here. Solving Eqs. (14)–(15) concurrently for the pressure gradients, and retaining terms to $\mathcal{O}(\epsilon^2)$, we find

$$\frac{\partial\tilde{\Pi}}{\partial\tilde{x}}\left[1-2\epsilon^2\frac{\partial\tilde{\eta}_s}{\partial\tilde{\Pi}}\frac{\partial\tilde{u}}{\partial\tilde{x}}-\frac{\epsilon^2}{\chi}\left(\frac{\partial\tilde{\eta}_s}{\partial\tilde{\Pi}}\right)^2\left(\frac{\partial\tilde{u}}{\partial\tilde{y}}\right)^2\right]=\tilde{\eta}_s\left(\frac{\partial^2\tilde{u}}{\partial\tilde{y}^2}+\frac{\epsilon^2}{\chi}\frac{\partial\tilde{\eta}_s}{\partial\tilde{\Pi}}\frac{\partial\tilde{u}}{\partial\tilde{y}}\frac{\partial^2\tilde{v}}{\partial\tilde{y}^2}\right) \tag{B1}$$

and

$$\frac{\partial\tilde{\Pi}}{\partial\tilde{y}}=\frac{\epsilon^2}{\chi}\left(\tilde{\eta}_s\frac{\partial^2\tilde{v}}{\partial\tilde{y}^2}+\frac{\partial\tilde{\eta}_s}{\partial\tilde{\Pi}}\frac{\partial\tilde{\Pi}}{\partial\tilde{x}}\frac{\partial\tilde{u}}{\partial\tilde{y}}\right), \tag{B2}$$

where

$$\chi=1-2\epsilon^2\frac{\partial\tilde{\eta}_s}{\partial\tilde{\Pi}}\frac{\partial\tilde{v}}{\partial\tilde{y}}. \tag{B3}$$

Under the assumption that

$$\epsilon^2\left|\frac{\partial\tilde{\eta}_s}{\partial\tilde{\Pi}}\right|\ll 1, \tag{B4}$$

these become, to leading order,

$$\frac{\partial\tilde{\Pi}}{\partial\tilde{x}}\left[1-\epsilon^2\left(\frac{\partial\tilde{\eta}_s}{\partial\tilde{\Pi}}\right)^2\left(\frac{\partial\tilde{u}}{\partial\tilde{y}}\right)^2\right]=\tilde{\eta}_s\frac{\partial^2\tilde{u}}{\partial\tilde{y}^2}, \tag{B5}$$

and

$$\frac{\partial\tilde{\Pi}}{\partial\tilde{y}}=0. \tag{B6}$$

Clearly, a stricter criterion than Eq. (B4) emerges:

$$\epsilon\left|\frac{\partial\tilde{\eta}_s}{\partial\tilde{\Pi}}\right|\ll 1. \tag{B7}$$

If Eq. (B7) holds, the condition in Eq. (B4) is patently true as well, and the lubrication equations simplify to the familiar Newtonian form of Eq. (19) (albeit with Π-dependent viscosity).

The condition in Eq. (B7) prevents $\partial\tilde{\Pi}/\partial\tilde{x}$ from diverging, per Eq. (B5). Bair et al. [24] noticed this divergence, and established a criterion for the validity of the lubrication equations with Π-dependent viscosity in terms of a condition on the maximum principal stress in the fluid. Setting $\partial\tilde{\eta}_s/\partial\tilde{\Pi}=\Pi_\ell/\Pi_c\tilde{\eta}_s$, Eq. (B7) is equivalent to (in dimensional units)

$$\tau_{\max}=\left|\eta_s(\Pi)\frac{\partial u}{\partial y}\right|_{\max}<\Pi_c. \tag{B8}$$

Therefore, Π_c sets an upper limit set on the shear stresses. We shall assume this is the case, and proceed with the simplified form of the lubrication equations. The validity of the stress criterion in Eq. (B8) is verified *a posteriori* for two representative cases below.

In pressure driven flow, the maximum stress condition becomes

$$\tau_{\max}=\frac{h}{2}\frac{\partial\Pi}{\partial x}\bigg|_{\max}<\Pi_c. \tag{B9}$$

Using Eq. (47) to estimate the maximum pressure gradient, we find

$$\frac{\partial\Pi}{\partial x}\bigg|_{\max}\approx\frac{\Pi_c}{L}\frac{1-e^{-\Delta\Pi/\Pi_c}}{e^{-\Delta\Pi/\Pi_c}}, \tag{B10}$$

which, when $\Delta\Pi \ll \Pi_c$, is the same condition found by Denn [21] in the flow of polymer melts in a capillary. In general, this condition prescribes an upper bound on the applied pressure drop $\Delta\Pi$ across the channel for which the simplified lubrication equations are valid:

$$\Delta\Pi \lessapprox \Pi_c \ln(L/h). \tag{B11}$$

For thin channels, therefore, the qualitatively new effects predicted for $\Delta\Pi \sim \Pi_c$ in Section III will still be valid before the stress condition in Eq. (B8) breaks down.

In the case of a disk approaching a wall, the maximum pressure gradient in the channel may be similarly estimated, and we find

$$\left.\frac{\partial\Pi}{\partial x}\right|_{\max} \approx \frac{\Pi_c}{L_{\text{circ}}} \frac{1}{\sqrt{1-V/V_m}}. \tag{B12}$$

The maximum shear stress condition now translates to

$$V \lessapprox V_m \left(1 - \frac{h_0}{8R}\right). \tag{B13}$$

The velocity of approach (or equivalently, the squeezing force) is not limited by the maximum value V_m predicted in Section IV, but by a corrected value at which the pressure gradient diverges. Again, for small gaps, this condition is only marginally more restrictive.

[1] L E Scriven and C V Sternling, "The marangoni effects," Nature **187**, 186–188 (1960).
[2] V G Levich and V S Krylov, "Surface-tension-driven phenomena," Annual Review of Fluid Mechanics **1**, 293–316 (1969).
[3] A E Hosoi and John W M Bush, "Evaporative instabilities in climbing films," J. Fluid Mech. **442**, 217–239 (2001).
[4] J R A Pearson, "On convection cells induced by surface tension," J. Fluid Mech. **4**, 489–500 (1958).
[5] Y. T. Hu, D. J. Pine, and L. Gary Leal, "Drop deformation, breakup, and coalescence with compatibilizer," Physics of Fluids **12**, 484–489 (2000).
[6] Gerald G. Fuller and Jan Vermant, "Complex fluid-fluid interfaces: Rheology and structure," Annual Review of Chemical and Biomolecular Engineering **3**, 519–543 (2012).
[7] D. Langevin, "Rheology of adsorbed surfactant monolayers at fluid surfaces," Annual Review of Fluid Mechanics **46**, 47–65 (2014).
[8] Carlton F Brooks, Gerald G Fuller, Curtis W Frank, and Channing R Robertson, "An interfacial stress rheometer to study rheological transitions in monolayers at the air-water interface," Langmuir **15**, 2450–2459 (1999).
[9] Tom Verwijlen, Paula Moldenaers, Howard A. Stone, and Jan Vermant, "Study of the flow field in the magnetic rod interfacial stress rheometer," Langmuir **27**, 9345–9358 (2011).
[10] Joseph R. Samaniuk and Jan Vermant, "Micro and macrorheology at fluid-fluid interfaces," Soft Matter **10**, 7023–7033 (2014).
[11] Zachary A. Zell, Arash Nowbahar, Vincent Mansard, L. Gary Leal, Suraj S. Deshmukh, Jodi M. Mecca, Christopher J. Tucker, and Todd M. Squires, "Surface shear inviscidity of soluble surfactants," Proc. Natl. Acad. Sci. USA **111**, 3677–3682 (2014).
[12] Zachary A. Zell, Vincent Mansard, Jeremy Wright, KyuHan Kim, Siyoung Q. Choi, and Todd M. Squires, "Linear and nonlinear microrheometry of small samples and interfaces using microfabricated probes," Journal of Rheology **60**, 141–159 (2016).
[13] L.E. Scriven, "Dynamics of a fluid interface equation of motion for newtonian surface fluids," Chemical Engineering Science **12**, 98 – 108 (1960).
[14] P. G. Saffman, "Brownian motion in thin sheets of viscous fluid," J. Fluid Mech. **73**, 593–602 (1976).
[15] P G Saffman and M Delbrück, "Brownian motion in biological membranes," Proceedings of the National Academy of Sciences **72**, 3111–3113 (1975).
[16] V. Prasad, S. A. Koehler, and Eric R. Weeks, "Two-particle microrheology of quasi-2d viscous systems," Phys. Rev. Lett. **97**, 176001 (2006).
[17] C. J. A. Roelands, J. C. Vlugter, and H. I. Waterman, "The Viscosity-Temperature-Pressure Relationship of Lubricating Oils and Its Correlation With Chemical Constitution," Journal of Basic Engineering **85**, 601 (1963).
[18] S. Bair and W. O. Winer, "The High Pressure High Shear Stress Rheology of Liquid Lubricants," Journal of Tribology **114**, 1 (1992).
[19] Richard L. Cook, H. E. King, Chris A. Herbst, and Dudley R. Herschbach, "Pressure and temperature dependent viscosity of two glass forming liquids: Glycerol and dibutyl phthalate," The Journal of Chemical Physics **100**, 5178 (1994).
[20] Richard C. Penwell, Roger S. Porter, and Stanley Middleman, "Determination of the pressure coefficient and pressure effects in capillary flow," Journal of Polymer Science Part A-2: Polymer Physics **9**, 731–745 (1971).

[21] Morton M Denn, "Pressure drop-flow rate equation for adiabatic capillary flow with a pressure- and temperature-dependent viscosity," Polymer Engineering and Science **21**, 65–68 (1981).

[22] J Hron, J. Malek, and K. R. Rajagopal, "Simple flows of fluids with pressure-dependent viscosities," Proceedings of the Royal Society A: Mathematical, Physical and Engineering Sciences **457**, 1603–1622 (2001).

[23] K. R. Rajagopal and A. Z. Szeri, "On an inconsistency in the derivation of the equations of elastohydrodynamic lubrication," Proceedings of the Royal Society A: Mathematical, Physical and Engineering Sciences **459**, 2771–2786 (2003).

[24] Scott Bair, Michael Khonsari, and Ward O. Winer, "High-pressure rheology of lubricants and limitations of the Reynolds equation," Tribology International **31**, 573–586 (1998).

[25] Rachel E Kurtz, Arno Lange, and Gerald G Fuller, "Interfacial rheology and structure of straight-chain and branched fatty alcohol mixtures," Langmuir **22**, 5321–5327 (2006).

[26] KyuHan Kim, Siyoung Q. Choi, Joseph A. Zasadzinski, and Todd M. Squires, "Interfacial microrheology of dppc monolayers at the air-water interface," Soft Matter **7**, 7782–7789 (2011).

[27] KyuHan Kim, Siyoung Q. Choi, Zachary A. Zell, Todd M. Squires, and Joseph A. Zasadzinski, "Effect of cholesterol nanodomains on monolayer morphology and dynamics," Proc. Natl. Acad. Sci. USA **110**, 3054–3060 (2013).

[28] Eline Hermans and Jan Vermant, "Interfacial shear rheology of dppc under physiologically relevant conditions," Soft Matter **10**, 175–186 (2014).

[29] Vladimir M Kaganer, Helmuth Möhwald, and Pulak Dutta, "Structure and phase transitions in langmuir monolayers," Rev. Mod. Phys. **71**, 779 (1999).

[30] Morrel H Cohen and David Turnbull, "Molecular transport in liquids and glasses," J. Chem. Phy. **31**, 1164–1169 (1959).

[31] Mark Sacchetti, Hyuk Yu, and George Zografi, "In-plane steady shear viscosity of monolayers at the air/water interface and its dependence on free area," Langmuir **9**, 2168–2171 (1993).

[32] Siyoung Q. Choi, Kyuhan Kim, Colin M. Fellows, Kathleen D. Cao, Binhua Lin, Ka Yee C. Lee, Todd M. Squires, and Joseph A. Zasadzinski, "Influence of molecular coherence on surface viscosity," Langmuir **30**, 8829–8838 (2014).

[33] William D Harkins and John G Kirkwood, "The viscosity of monolayers: Theory of the surface slit viscosimeter," The Journal of Chemical Physics **6**, 53 (1938).

[34] Daniel K. Schwartz, Charles M. Knobler, and Robijn Bruinsma, "Direct observation of langmuir monolayer flow through a channel," Phys. Rev. Lett. **73**, 2841–2844 (1994).

[35] H A Stone, "Fluid motion of monomolecular films in a channel flow geometry," Phys. Fluids **7**, 2931–2937 (1995).

[36] M. L. Kurnaz and D. K. Schwartz, "Channel flow in a langmuir monolayer: Unusual velocity profiles in a liquid-crystalline mesophase," Phys. Rev. E **56**, 3378–3384 (1997).

[37] A Relini, F Ciuchi, and R Rolandi, "Surface shear viscosity and phase transitions of monolayers at the air-water interface," Journal de Physique II **5**, 1209–1221 (1995).

[38] Howard A Stone, Abraham D Stroock, and Armand Ajdari, "Engineering flows in small devices: Microfluidics toward a lab-on-a-chip," Annu. Rev. Fluid Mech. **36**, 381–411 (2004).

[39] Patricia Burriel, Josep Claret, Jordi Ignés-Mullol, and Francesc Sagués, ""bottleneck effect" in two-dimensional microfluidics," Phys. Rev. Lett. **100**, 134503 (2008).

[40] L Gary Leal, *Advanced transport phenomena* (Cambridge University Press, 2007).

[41] G. K. Batchelor and J. T. Green, "The hydrodynamic interaction of two small freely-moving spheres in a linear flow field," J. Fluid Mech. **56**, 375–400 (1972).

[42] Frank Snijkers, Rossana Pasquino, and Jan Vermant, "Hydrodynamic interactions between two equally sized spheres in viscoelastic fluids in shear flow," Langmuir **29**, 5701–5713 (2013).

[43] G. J. Elfring, L. G. Leal, and T. M. Squires, "Surface viscosity and marangoni stresses at surfactant laden interfaces," J. Fluid Mech. **792**, 712–739 (2016).

[44] Zachary A. Zell, Lucio Isa, Patrick Ilg, L. Gary Leal, and Todd M. Squires, "Adsorption energies of poly(ethylene oxide)-based surfactants and nanoparticles on an airwater surface," Langmuir **30**, 110–119 (2014).

[45] Valeria Garbin, Ian Jenkins, Talid Sinno, John C. Crocker, and Kathleen J. Stebe, "Interactions and stress relaxation in monolayers of soft nanoparticles at fluid-fluid interfaces," Phys. Rev. Lett. **114**, 108301 (2015).

[46] Valeria Garbin, John C. Crocker, and Kathleen J. Stebe, "Forced desorption of nanoparticles from an oil-water interface," Langmuir **28**, 1663–1667 (2012).

[47] Howard A Stone and Armand Ajdari, "Hydrodynamics of particles embedded in a flat surfactant layer overlying a subphase of finite depth," J. Fluid Mech. **369**, 151–173 (1998).

[48] Th. M. Fischer, "The drag on needles moving in a Langmuir monolayer," J. Fluid Mech. **498**, 123–137 (2004).